Effect of carbons' structure and type on AC electrical properties of polymer composites: Predicting the percolation threshold of permittivity through different models

Mostafizur Rahaman[1]*, Prashant Gupta[2], Mokarram Hossain[3], Govindasami Periyasami[1], Paramita Das[4]

[1]Department of Chemistry, College of Science, King Saud University, P.O. Box 2455, Riyadh 11451, Saudi Arabia

[2]MIT-Centre for Advanced Materials Research and Technology(M-CAMRT), Department of Plastic and Polymer Engineering, Maharashtra Institute of Technology, Aurangabad 431010 Maharashtra

[3]Zienkiewicz Centre for Computational Engineering, College of Engineering, Swansea University, SA1 8EN, United Kingdom

[4]Department of Chemical Engineering, Indian Institute of Science Education and Research Bhopal, Bhopal 462066, Madhya Pradesh, India

***Corresponding author email id**: mrahaman@ksu.edu.sa (MR)

Abstract

The AC electrical properties of EVA and NBR based composites filled with different conductive fillers were investigated. Result shows several magnitude increment in AC electrical conductivity and dielectric permittivity after addition of these conductive fillers: indicating that these materials can be used as supercapacitors. The magnitude of increment was varied according to polymer and filler types. Herein, we also have tested the applicability of different Sigmoidal models to find out the percolation threshold value of permittivity for these binary polymer composite systems. It is observed that except Sigmoidal–Boltzmann and Sigmoidal–Dose-Response models, other Sigmoidal models exhibit different values of percolation threshold when considered for any particular polymer composite system. The paper discusses the variation in results of percolation threshold with an emphasis on the advantages, disadvantages, and

limitations of these models. We also have applied the classical percolation theory to predict the percolation threshold of permittivity and compared with all the reported sigmoidal models. To judge the unanimous acceptability of these models, they were tested vis-à-vis the permittivity results of various polymer composites reported in published literature. To comprehend, all the models except the Sigmoidal-Logistic-1 model were successfully applicable for predicting the percolation threshold of permittivity for polymer composites.

Keywords

Polymer composites, dielectric constant, percolation threshold, sigmoidal models, classical percolation theory

Introduction

Polymers are versatile and thus find their use in numerous domestic and industrial applications. One of the major application areas includes electrical and electronics due to their high electrical breakdown, low dielectric loss, ease in processing, and lower cost[1]. A host of conductive polymers such as polypyrrole, polyaniline, polythiophene, and their derivatives reportedly have a high value of dielectric constant/permittivity[2]. However, most of other polymeric materials exhibit low permittivity as they are generally non-conductive in nature. To improve their functionality in such applications, a great deal of research is carried out on the incorporation of high dielectric constant fillers into the non-conductive polymeric matrices. One such extensively researched material, ceramic has good electrical characteristics but is extremely porous, dense, and rigid[3–5]. Some other fillers have reported improvements regarding this functionality include $BaTiO_3$[6, 7], graphite[8], carbon nanotube (CNT)[7], silica[8], and a host of metallic fillers based on Ni, Ca, Cu, Ag, etc[9, 10], leading to the formation of polymer matrix composites reporting high dielectric properties. In addition to the above fillers, carbon-based particulate[11] and fibrous[12] fillers have gained importance due to better electrical properties such as permittivity and dielectric loss, which is evident by the transition of the material from insulator to conductor above the percolation threshold. Dielectric polymer composites with high permittivity and low loss have great applicability in energy storage[13] and energy

harvesting[14] applications. Maheswar Panda reported the percolative and non-percolative phenomena in polymer dielectric composites in his published book[15]. Electrical, dielectric, rheological, morphological properties of polymer composites were discussed in the light of theoretical modelling and spectroscopic point of views. The polymer composites were suitable for energy storage devices.

The formation of induced electric dipoles along with permanent dipoles are observed as they align themselves with respect to an externally applied field. This dipole alignment results in polarization, a material constant that depends on the externally applied electrical field. The electronic and ionic charges undergo displacement into the bulk of material due to the externally applied field, which on the contrary, returns to its normal state after its withdrawal. A parameter independent of the strength of the electric field, i.e., permittivity, is used for dielectric characterization of any material. It depends upon the number of dipoles in the material, its strength, temperature, and frequency[16].

The percolation phenomena of polymer/metal dielectrics were also studied [17–21]. In these articles, the authors have discussed the effect of process conditions, polymer matrix, surface and interface of filler particles on percolation threshold and non-universal scaling behavior of polymer-nickel composites near percolation threshold. There are abundant literatures available on the determination of permittivity of polymer composites but discussions over its percolation threshold trends have not been done. Like electrical conductivity, the percolation threshold for permittivity can also be mathematically determined using either classical percolation theory or different Sigmoidal models.

In this article, we have reported the effects of type of conductive carbon fillers on the AC electrical and dielectric properties with respect to fillers loadings, polymer type, and frequency of electric field. Moreover, the current investigation is also concerned with determining the percolation threshold of dielectric permittivity for the first time using different Sigmoidal models and classical percolation theory. We have also tried, herein, to validate these models for other polymer composites as well. We have selected two types of polymers and three types of carbon fillers for the complete validation of this study.

Methodologies

Materials

Ethylene vinyl acetate (EVA) copolymer and acrylonitrile butadiene rubber (NBR) were used as the base polymeric materials. NBR-33 and EVA-2806 had mooney viscosity (ML_{1+4}) at 100 °C of 45.0 and 20.0, respectively. EVA had 28.0 percent vinyl acetate content and 6.0 g/10 mins MFI. Both polymers were procured from Japan Synthetic Rubber Co. Ltd, NOCIL, Mumbai, India. We have used three conductive carbon fillers as mentioned earlier: two of them are particulate fillers and another one is fibrous filler. The particulate fillers, namely, conductex (SC Ultra bead) carbon black (CCB) and printex XE2 carbon black (PCB) have been procured from Columbian Chemicals Company-Atlanta, Degussa Canada Limited. On the other hand, the fibrous filler, short carbon fibers (SCF) has been supplied by R K Carbon Fiber Leatherhead, UK. The curing agent used in the composite, i.e., dicumyl peroxide (DCP), 98.0 % purity with a melting point of 80.0 °C was obtained from Aldrich Chemicals Company, USA. Moreover, we have used a co-vulcanizing agent (tri-allyl-cyanurate, TAC) and an anti-oxidant (1,2-dihydro-2,2,4-trimethylquinolone, TQ) for the better performance of the composites and their longevity. The former one has been procured from E. Merck (India limited), India; whereas, the latter on from Lanxess (India) Private Ltd.

Method of composite preparation

The compounding of EVA/carbon blacks and NBR/carbon blacks' composites was done using both internal and external mixers. We used Brabender Plasticorder (PLE 330, Brabender GmbH & Co. KG, Duisburg, Germany) as an internal mixer where the individual polymers were melted at 120 °C, for mixing time 6 mins and at 60 rpm to make a compacted mass. The mixing of carbon black fillers and other necessary co-ingredients with the base polymers were performed externally at normal temperature using a two-roll mill (Santec Exim Pvt Ltd., Manesar, India). The ingredients were added sequentially according to the formulation provided in Table 1. On the other hand, a Haake Rheocord was used for compounding of short carbon fibers maintaining the same mixing condition that is at 120 °C for mixing time 6 mins and at 60 rpm. We had taken the fillers' quantity as per weight of hundred parts of polymer (phr). Its quantity as the volume fraction (V_f) are also given in Table 1. A Monsanto rheometer R-100S (Gomaplast Machinery,

Inc., OH, USA) was used to determine the curing time of various composites at 160 °C for 1 hr. Lastly, the composites were cured at temperature 160 °C within a compression mold as per their calculated curing time.

Table 1 Formulations of different composites based on various fillers

Ingredients	Composition in phr and V_f of fillers in polymer			
	E_0N_{100} (phr)	**E_0N_{100} (V_f)**	**$E_{100}N_0$ (phr)**	**$E_{100}N_0$ (V_f)**
EVA	0	-	100	1
NBR	100	1	0	-
DCP	02	0.02	02	0.02
TAC	01	0.01	01	0.01
TQ	01	0.01	01	0.01
CCB	0, 10, 20, 30, 40, 50, 60	0, 0.051, 0.096, 0.139, 0.178, 0.213, 0.245	0, 10, 20, 30, 40, 50, 60	0, 0.051, 0.096, 0.139, 0.178, 0.213, 0.245
PCB	0, 10, 20, 30, 40, 50	0, 0.051, 0.096, 0.139, 0.178, 0.213	0, 10, 20, 30, 40, 50	0, 0.051, 0.096, 0.139, 0.178, 0.213
SCF	0, 5, 10, 15, 20, 25, 30	0, 0.026, 0.051, 0.075, 0.096, 0.119, 0.139	0, 5, 10, 15, 20, 25, 30	0, 0.026, 0.051, 0.075, 0.096, 0.119, 0.139

Alpha numerical codes were used to designate the samples when used in figures and tables. The composites are designated as XY or XYZ, where, X is indicating the polymer, Y is filler, and Z is filler's quantity. EVA was designated as E, NBR as N, CCB as C, PCB as P, and SCF as F.

Experimental measurements

We measured the AC electrical conductivity (σ), dielectric constant (ε′) and loss (ε″) of the composite materials. These AC electrical properties were tested the use of an LCR meter (Quadtech 7600) over the frequency range 10-10^6 Hz. To measure it, we use a home-made electrode. The diameter of electrode was 1.2 cm. The testing was performed as per ASTM D150. The data was selectively used for the determination of percolation threshold of dielectric

constant/permittivity at the frequency of 1 MHz. The permittivity of the composite materials was calculated as, permittivity ε' = (C * t)/ 0.0885 A. In this equation, *C* refers to capacitance of sample in pico farad, *t* refers to the thickness in centimeter, and *A* refers to area in cm^2.

Results and discussion

AC electrical conductivity

The effect of frequency on AC conductivity (σ) of polymer based composites filled with various types of carbon fillers namely CCB, PCB, and SCF have been shown in Figs. 1. It is found from these figures that the σ has continuously increased as the frequency proceeds from its low value to high value for the low filler loaded composites. At lower filler loading, the filler particles remain isolated within the matrices. Hence, the phenomena of increase in σ with increment in frequency cannot be explained with the theory of the general mechanism of conduction, rather it can be attributed to the hopping mechanism of conduction theory. As frequency is increased, the electrons present in the conductive ingredients get more and more energized and excited, thereby leading to its hopping through the adjacent conductive sites. With the progressive increase in frequency, this tendency of hopping electrons through the adjacent conductive sites is increased, resulting in a greater number of charge carriers flowing through the composite system. As a result, the σ is observed to increase when the frequency is proceeded from its low to high value for the low filler loaded composite systems[22]. However, the composites with higher filler loading behave almost independently of frequency. The key factor for the rise in σ with frequency is the hopping mechanism of conduction as explained earlier. This hopping phenomenon is in effect when the particles are not in direct contact with each other. At high loading, because of formation of continuous conductive networks, the electrons flow directly through these networks, and consequently, the conduction through hopping becomes insignificant. Hence, the net AC conduction is entirely due to normal DC conductivity through the continuous conductive chain. This attributes to the frequency independent behavior for the composites having higher loading of filler particles.

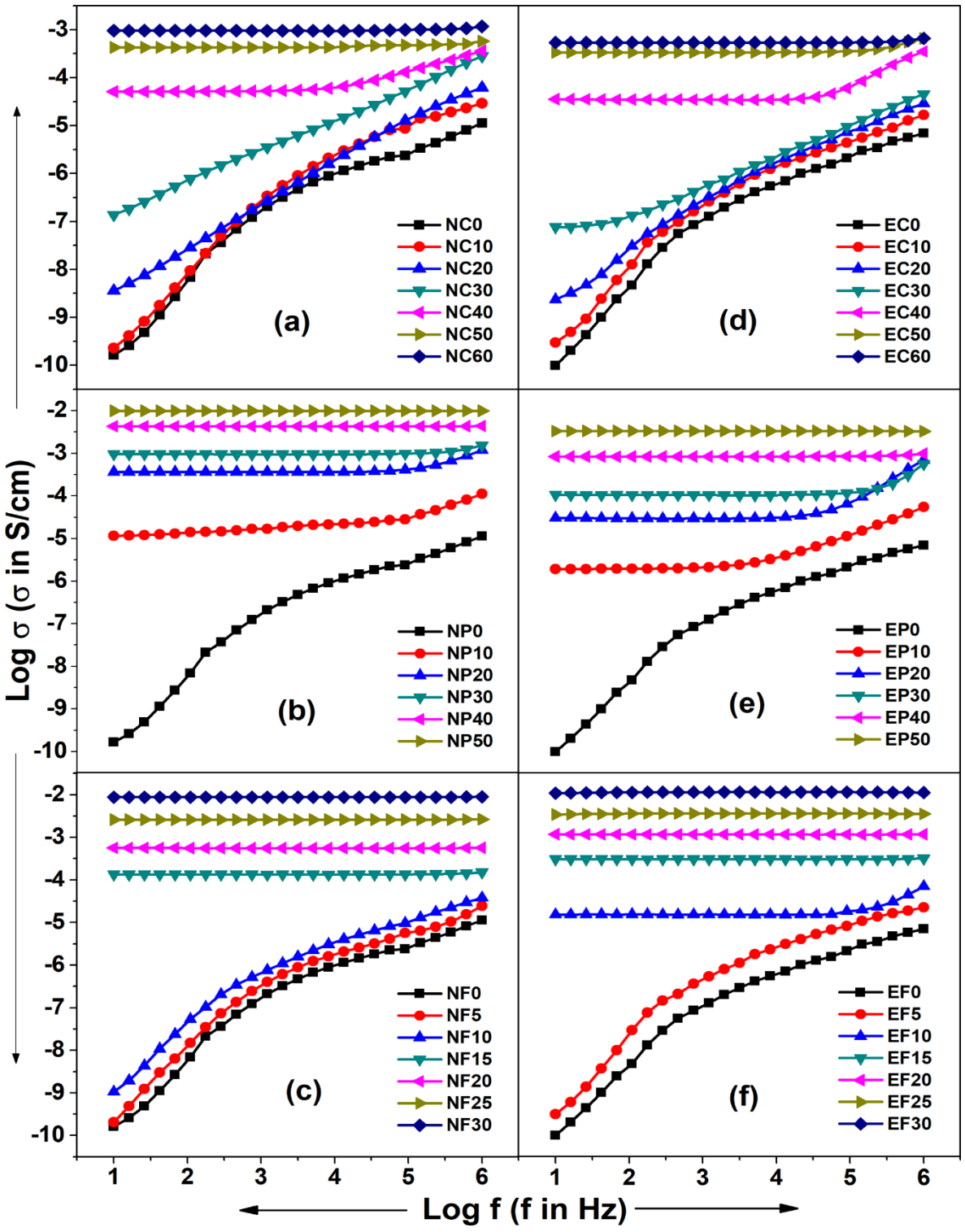

Fig. 1 AC conductivity vs frequency of NBR and EVA based composites loaded with CCB, PCB and SCF.

It is also observed from the figures that at a certain frequency, the σ has increased against the filler loading for all the composite systems. In the case of insulating polymers, the charge carriers are localized, where the electrical transport is because of the hopping of charge carriers. With the addition of conductive fillers, the charge carriers get their path to flow and become delocalized. The magnitude of delocalization of charge carriers increases as the filler loadings is increased. Consequently, the σ also increases with the variation in fillers' loadings to its higher value. Beyond a certain loading, i.e., where the conductivity becomes frequency independent, the fillers form a continuous conductive network within the polymer matrices. Hence, the delocalization of charge carriers is facilitated beyond this loading of fillers.

The figure shows that the carbon fiber filled composites (except EVA/fiber composite) exhibit higher conductivity compared to Printex black filled systems followed by Conductex black at their equal loadings. This is because, the dimension of fillers being quite different from each other. Fillers' physical properties are given in Table S1 and S2, and Figure S1 of the supplementary section. It is envisaged from Table S2 and Figure S1 that the aspect ratio of SCF is high enough compared to the both carbon blacks. As a result, carbon fiber forms conductive channel through the polymer matrices more easily at lower loading of fillers. Hence, carbon fiber filled composites show higher electrical conductivity compared to particulate blacks filled composites. Structurally, PCB is higher compared to CCB. Higher structure of black facilitates the formation of conductive channels through the polymer matrices. As a result, PCB filled composites showed higher σ than that of CCB filled composites at their similar filler loading.

It is revealed from the Figure 1 that NBR based composites exhibit higher σ than that of EVA based composites at their equal carbon blacks' loading and frequency. The mixing of both carbon blacks with these two polymers have been carried out at normal temperature. As NBR is an elastomer, hence the breaking carbon particles structure during mixing with it is less compared to mixing with EVA. This cleavage of the structure reduces the size of carbon particles, which make it less favorable to form conductive channels through the host medium. So, the σ of EVA-carbon blacks based composites becomes less than that of NBR-carbon blacks based composites at similar filler loading. However, in case of fiber filled composites, opposite trend is observed. This is due to the fiber being mixed with both polymers at high temperature (120 °C). At such temperatures, EVA exhibits a softer phase than NBR. Obviously, in this case,

the breaking of fiber within NBR matrix during mixing will be more compared to EVA. This resulted the high value of σ of EVA-fiber composites than that of NBR-fiber composites at their equal fiber loading.

Dielectric properties

The variation of ε′ and ε″ with respect to frequency have been shown in Figs. 2 and 3 for polymer based composites loaded with various carbon fillers. The figures show that both the ε′ and ε″ for the composites with lower filler loading behave almost frequency-independently for all the systems under investigation. However, the value of ε′ and ε″ are decreasing for all the composites, having higher loading of conductive fillers when the frequency is proceeded from its lower to higher value. The value of ε′ and ε″ of composite systems depend on various polarization effects brought about by the application of an alternating electric field, such as electronic polarization is caused by the presence and orientation of electrons, and atomic polarization is caused by atoms, polar and non-polar groups. The interface between the polymer matrix and the filler particles also experiences interfacial polarization. The most significant property that influences the dielectric property of composite systems containing various conductive particles in an insulating polymer matrix is the effect of interfacial polarization. Over low frequency range, the dipoles of the polymer composite systems have enough time to align themselves with the applied electric AC field. Consequently, the effect of polarization, especially interfacial polarization, is greater over low frequency range and lessens as frequencies rise because the dipoles have so little time to orient themselves. The effect of polarization will cause an increase in the dielectric properties. Consequently, there is the fall of dielectric properties while the frequency rises[23].

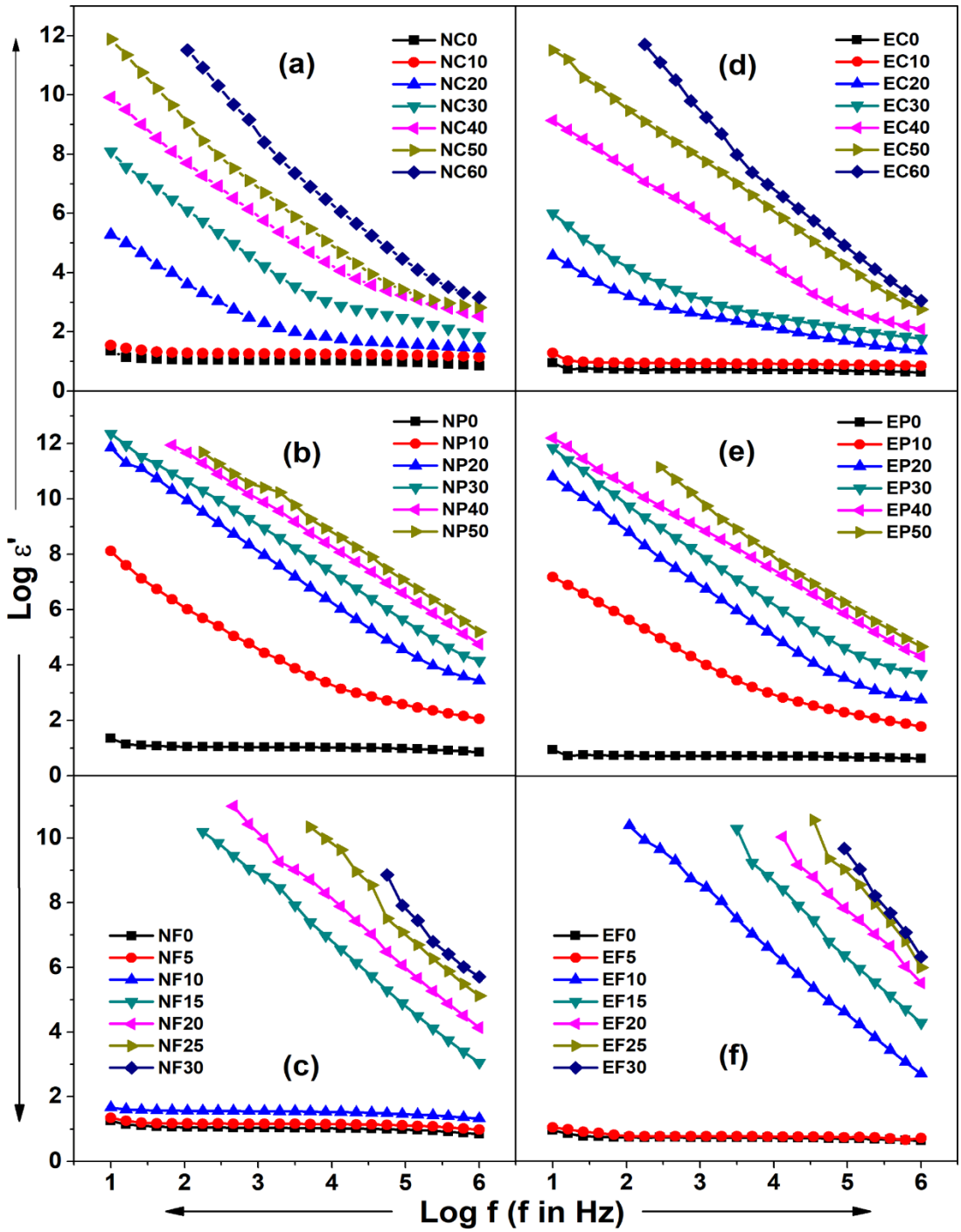

Fig. 2 Dielectric constant vs frequency of NBR and EVA based composites loaded with CCB, PCB and SCF.

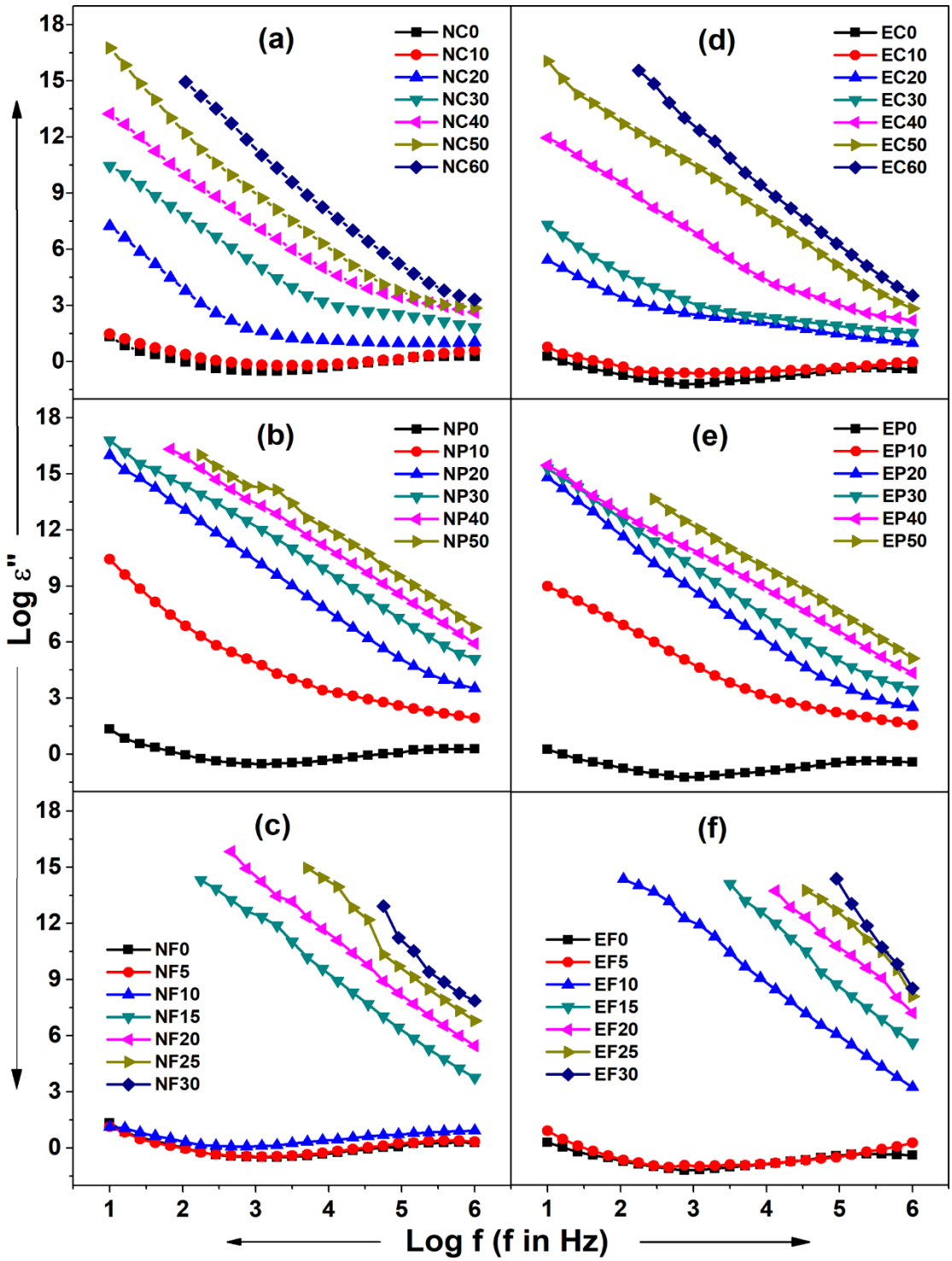

Fig. 3 Dielectric loss vs frequency of NBR and EVA based composites loaded with CCB, PCB and SCF.

The figures also show that, at a certain frequency, the value of both ε′ and ε″ has sufficiently improved after the increase in filler loadings. This is observed for all the composite systems. The added filler particles within the polymers act as micro capacitors. This is because of the presence of insulating polymer in between two conductive particles acting as electrodes. Further, the carbon black particles are associated with many polar groups such as –COOH, –CHO, –OH, –CO–, etc. on their surfaces act as different dipoles. When carbons' concentration are increased, the number of such micro capacitors is increased[22]. Initially, that is at low level of carbon loading, the capacitors are separated from one another and hence the increase in dielectric properties are only due to the increase in their number in quantity. Adding more quantity of carbon to the polymer matrix, the conductive particle aggregates form big clusters in different size and shape, and finally make continuous conducting networks with clusters of infinite size. With the increase in conductive filler, the average gap between filler particles decreases, that is insulation thickness decreases in between electrons, which increases the capacitance of the capacitor.

The points to be noted herein is that, with increasing the quantity of carbon, the numbers as well as charge storage ability of the capacitors are increased. This has resulted further increment in interfacial polarization and hence the improvement in capacitance value of the composite systems with increasing in carbons' quantity, which in turn increases the dielectric constant and loss. The high value of ε″ compared to ε′ for the filled composite systems at a particular filler loading is mainly because of high value of dissipation factor, which is many fold greater than unity.

The effect of frequency on ε′ and ε″ of EVA and NBR based composites filled with 30 phr CCB, PCB, and SCF has been shown in Fig. 4. The figures exhibit that the ε′ and ε″ of NBR composites are higher compared to their EVA counterparts at the equal level of carbon blacks' loading for both composites; whereas, SCF filled composites exhibit reverse trend, that is, the dielectric properties are higher for composites made from EVA compared to composites made from NBR. The mixing of carbon blacks has been carried out at room temperature, where EVA has higher viscosity because of its thermoplastic elastomeric nature compared to relatively softer elastomer NBR. Therefore, due to higher viscosity of EVA than that of NBR (at the mixing temperature in between 45–50 °C), the shear force exerted on the particulate aggregate during

mixing is higher for EVA composites compared to NBR ones. The higher the shearing force exerted on the black particles; the higher will be the extent of breakdown of their structure (aggregate) in the polymer matrices. Therefore, the size and shape of the carbon black aggregates is reduced to a greater extent in EVA composites compared that in NBR ones. Thus, the micro capacitors made from carbon black–polymer–carbon black has lower capacitance in EVA composites compared to similar micro capacitors formed in NBR composites, which consequently lead to lower value of ε' and ε''. On the contrary, the carbon fiber has been mixed with the polymer matrices at 120 °C. At this temperature, the viscosity of EVA composites is lower than that of NBR one. Accordingly, the breakdown of fibers is more in NBR composites, which leads to the lower value of their dielectric properties.

A careful look into the Fig. 4 reveals that the dielectric properties of CCB, PCB, and short carbon fiber filled composites are different at their equal filler loading. The order of decreasing the dielectric properties are short carbon fiber filled composites> Printex black filled composites> Conductex black filled composites. It is clarified earlier that the dielectric properties depend on shape and size of filled particle, filler loadings, characteristics of the matrix polymer, and frequency of AC electric field. Besides these, dielectric property also depends on the conductivity of filled particles. Higher the conductivity of the filled particle, higher will be its dielectric property. The size and conductivity of the filler particles are decreasing according to the order that is short carbon fiber> Printex black> Conductex black. SCF may be considered as several aggregates of carbon black particles. Moreover, PCB has higher structure than CCB. In this respect, SCF can be considered as several aggregates of capacitors made from carbon black particles. Therefore, carbon fiber filled composites exhibits higher dielectric constant and loss compared to carbon black filled systems at equal loading. Similarly, Printex black filled composites exhibits higher dielectric properties than that of CCB filled systems due to their higher structure.

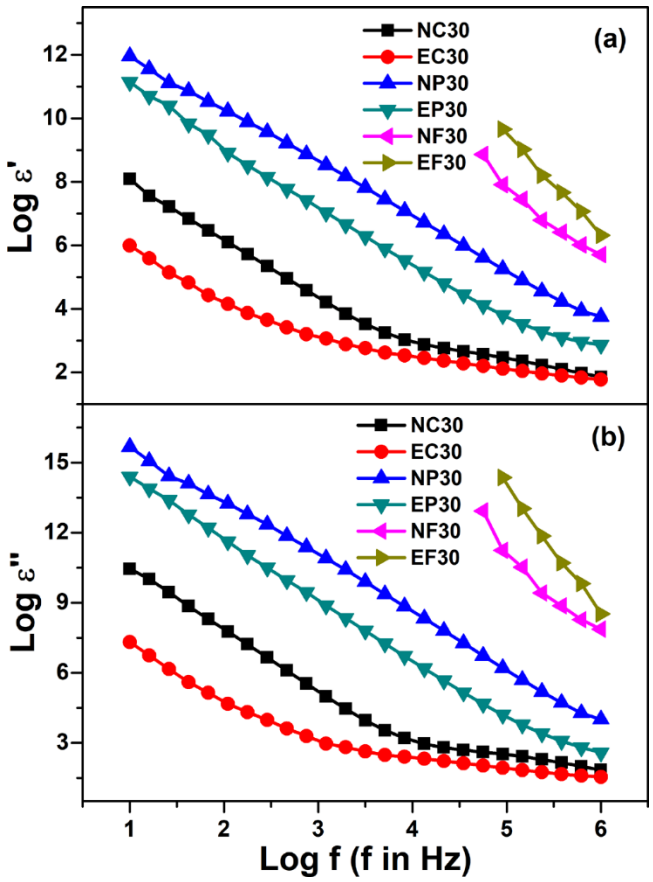

Fig. 4 (a) Dielectric permittivity and (b) dielectric loss vs frequency of EVA and NBR based composites at their 30 phr loadings.

Determination of percolation threshold of permittivity

The percolation threshold (P_t) of permittivity has been determined by various Sigmoidal models and classical percolation theory. These are discussed one-by-one within the following sections.

Sigmoidal-Boltzmann (SB) model

The SB model was reportedly employed for the study of spreading of Covid-19 virus waves[24]. In addition to it, it has also been used for understanding the energy bandgap of semiconductors[25], applicability of atmospheric pressure plasma jets in medicine[26], modelling of chemical parameter in pseudo binary alloys from the shift of the X-ray Bragg's angle[27], describe second peak in magnetization loops[28], etc.

The Sigmoidal Boltzmann model can be shown with the equation given as follows:

$$Y = A_2 + \frac{A_1 - A_2}{1 + e^{\left(\frac{x - x_0}{\Delta x}\right)}} \quad \text{.....(1)}$$

where Y is the permittivity at carbons' loading x of various carbons and is the independent variable; the initial (base polymer) and final (highest filler loading) values of permittivity are represented by the respective A_1 and A_2; Δx is the inclination of X-Y plot; and x_0 is evaluated as the X-axis point corresponding to its Y-axis point, mathematically expressed by $(A_1+A_2)/2$, i.e., the percolation threshold.

Upon differentiating equation 1, we get:

$$\frac{dy}{dx} = \frac{(A_2 - A_1)\, e^{\left(\frac{x - x_0}{\Delta x}\right)}}{\Delta x \left(1 + e^{\left(\frac{x - x_0}{\Delta x}\right)}\right)^2} \quad \text{.....(2)}$$

Equation 2 is the first order differentiation and will generate a maximum as shown in Fig. 5(a). Its magnitude can be attained by equalizing the d^2y/dx^2 to a zero value, which can alternatively be expressed as $x = x_0$. Hence, in Eq.1, x_0 resembles the P_t of permittivity. The use of same methodology can help in determining the point at which the P_t lies for other sigmoidal values as well, which has been detailed in different sections.

The percolation threshold of permittivity for both polymers matrix composites with various carbon fillers that is CCB, PCB, and short carbon fiber obtained through the Sigmoidal-Boltzmann model is shown in Fig. 5b, c, and d, respectively. Permittivity helps in the understanding of the effect of polarization and exhibits the ability of the material to align itself towards the electric field[29]. The ε' of polymeric composite materials, having conductive additives are considered as a mixer of huge number of micro-capacitors constituted of numerous conductive filler particles that are apart from one another by a thin non-conducting polymer layer. Hence, these types of heterogeneous systems can function as capacitors with magnificent dielectric properties capable of high charge storage[30]. Table 2 shows the value for all physical quantities need to figure out the permittivity. It is observed that the percolation threshold of NBR/CCB, EVA/CCB, NBR/PCB, EVA/PCB, NBR/SCF, and EVA/SCF based composites are 0.152±0.010, 0.157±0.003, 0.054±0.025, 0.062±0.009, 0.082±0.004, and 0.060±0.003,

respectively. This is indicating that the percolation threshold is high for composites filled with CCB when compared with PCB. The variation in percolation threshold among different series of composites can be explained by considering the structural/microstructural fact of conductive fillers. The structural images of these fillers and their selected composites are shown in the figure of Supplementary section S1. It is observed from this figure that the structure of printex black is high compared to conductex black. It means higher BET (Brunauer–Emmett–Teller) surface area of printex black in comparison to conductex black leads to a higher accumulation of charges within the filler. Moreover, a high structured carbon black may be considered as a combination of some capacitors of low structured carbon black. As a result, printex black filled composites has shown low percolation threshold of permittivity compared to conductex black filled composites. It can also be said that carbon black tends to form primary and secondary structures i.e., strong carbon aggregates. A higher structure in such a scenario is considered to be of a carbon aggregate possessing a more intricate dimension, shape, and internal void. Based on the statistical thickness method (STSA), the surface area of conductex black and printex black are 125 m^2/g and 587 m^2/g, respectively. Also, the understanding of a higher carbon structure is passively understood through the amount of dibutyl phthalate absorption by the filler particle. The absorption value reported for CCB and PCB is 115 cc/100 gm and 315-410 cc/100 gm, respectively. The values of permittivity in composites filled with various carbon forms are dependent upon the mixing viscosities of the polymers' matrices. Because of lower viscosity of NBR, the shear generation during mixing of polymer and filler will result in a lower breakdown of filler aggregates as mentioned earlier. On the contrary, the higher viscosity of EVA leads to more breakdown of the carbon black structure. This results in better dispersion but isolation in the polymer matrix thereby requiring a higher amount of filler requirement for polarization and a higher value of percolation threshold for dielectric permittivity[31]. The rate of orientation of a dipole towards the external electric field is maximum at the percolation threshold. This trend, however, changes in short carbon fiber-filled composites as the percolation threshold is observed at a lower volume fraction in EVA based composites when compared with NBR based composites. It is due to the processing methodology employed for the dispersion of short carbon fibers. The fibers were dispersed in the polymer matrix using an internal mixer at a temperature 120 ºC for 6 mins which was different from using a two-roll mill at a temperature of 45-60 ºC for

CCB and PCB filled polymer composites. It is pertinent to note that the temperature of mixing for short carbon fiber was almost two times higher compared to two-roll mill mixing process. EVA melts around 70-80 °C and the mixing of fibers with it was performed at 120 °C. Obviously, there was sufficient decrease in viscosity of EVA at its mixing temperature compared to NBR. This decrease in viscosity resulted in higher fiber length and aspect ratio of SCF in EVA composite than NBR composite. Herein, comparatively, high sharing force was exerted on fibers when mixed with NBR and resulted in low value of fiber aspect ratio.

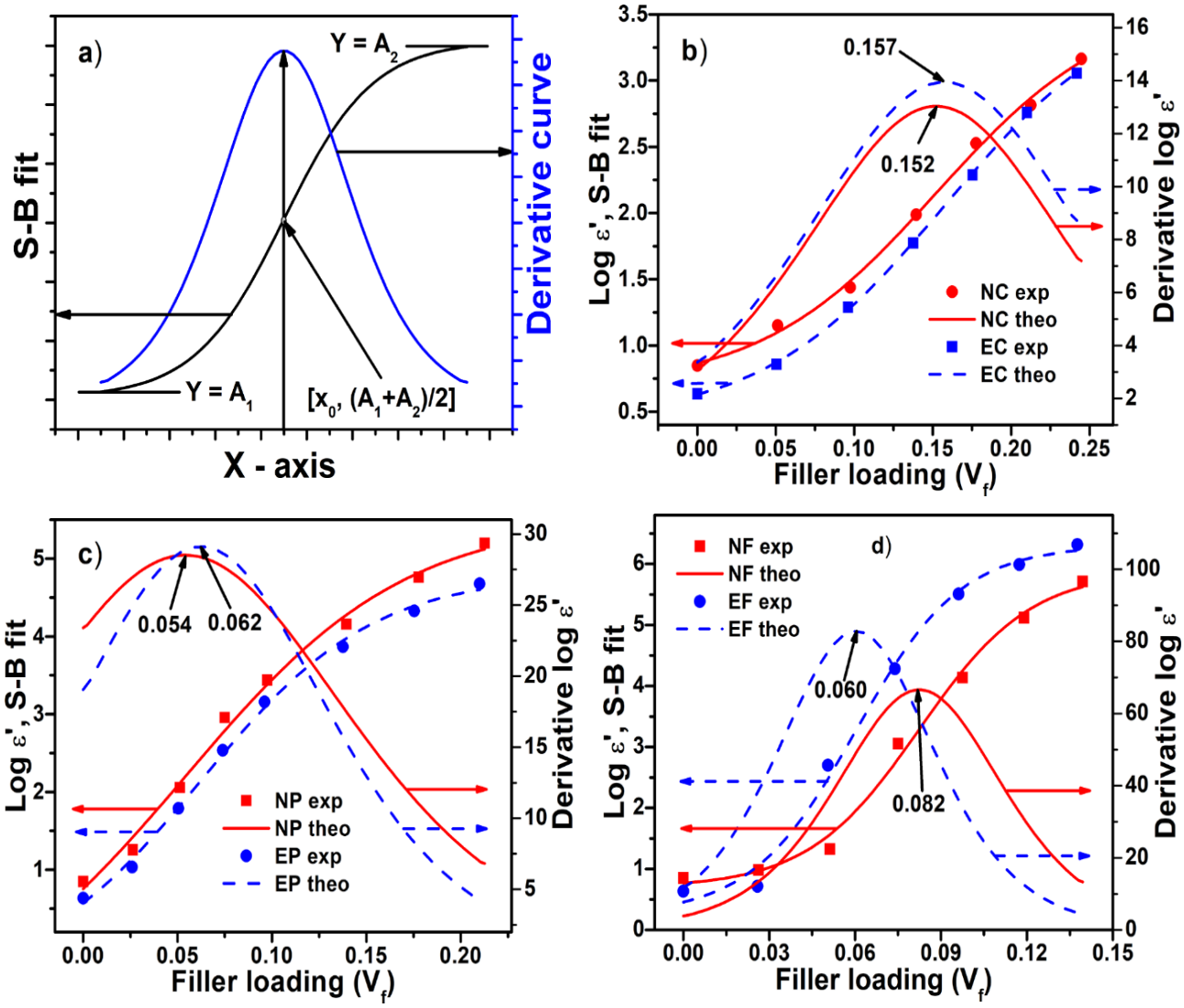

Fig. 5 Plots of (a) ideal curve (b) NC and EC composites (c) NP and EP composites, and (d) NF and EF composites based on experiment, theory and derivation as per SB model

Table 2 Extracted data as per SB model

SI	A_1	A_2	x_0	Δx	R^2
NC	00.68±0.14	3.61±0.28	0.152±0.010	0.056±0.011	0.995
EC	00.42±0.04	3.68±0.11	0.157±0.003	0.058±0.003	0.999
NP	00.14±0.03	5.54±0.43	0.054±0.005	0.059±0.019	0.991
EP	00.09±0.02	4.80±0.17	0.062±0.009	0.046±0.008	0.995
NF	00.69±0.14	5.88±0.37	0.082±0.004	0.019±0.004	0.987
EF	00.24±0.07	6.30±0.26	0.060±0.003	0.018±0.003	0.988

An increase in permittivity has been noticed after increase in filler loadings for all frequencies. The dielectric properties of both NBR and EVA are largely due to electronic polarization. In addition to the same, the carbon fillers within the composites function as dipoles, which can potentially work as micro-capacitors, leading to interfacial polarizations. A further increase in the filler content increase the quantity of such dipoles functioning as polar sites, and thereby, resulting in an improvement in permittivity with filler loading[32–34].

The aspect ratio of short carbon fiber (average length = 0.120 mm and diameter = 6.80 µm) was measured from optical microscopy images of SCF composites as shown in the image of Supplementary section S1. High aspect ratio of SCF is responsible for its lower percolation threshold than conductex black and comparable values to printex black[35]. The carbon fiber can be considered as a series of several capacitors made up of carbon particles[23]. It works as a milli-capacitor responsible for interfacial polarization[36]. An increase in the short carbon fiber loading increases the number of such capacitors resulting in a higher magnitude of polarization. This ultimately results in increased permittivity values with an increase in the filler loading[23, 37]. Also, below the values of percolation threshold, rate of orientation of dipoles towards the electric field is not at its peak value and hence, no major changes in the permittivity are observed. However, the dielectric values go up after the percolation threshold, resulting in a denser formation of the structure that will yield more charge accumulation.

Table 2 exhibits the data of parameters associated with SB model. Ideally, the value of R^2 should be unity with no error for the rest parameters. In this condition, the theoretical and experimental curves will superimpose on each other and show the perfect validation of the model. The data show that there is less deviation of R^2 and it is close to unity. Hence, it can be

inferred that the SB model is extremely valid to determine the percolation threshold of dielectric permittivity under discussion[38].

Sigmoidal-Dose Response (SD or SDR) model

The SDR model have been reportedly used in many applications such as ascertaining the correct dosage for radiation-induced urgency syndrome after gynecological radiotherapy[39], cardiovascular diseases[40], study the effects of nano-Ag and $AgNO_2$ on enzymatic and microbial action in calcareous soils[41], and to identify antiviral drugs against SARS-CoV-2[42]. This model equation is given as below:

$$Y = A_1 + \frac{A_2 - A_1}{1+10^{(\log x_0 - x)P}} \quad \text{.....(3)}$$

where x is the filler dosage volume fraction, log x_0 is a halfway between A_1 and A_2 which represent the initial (base polymer) and final (highest filler loading) values of permittivity, respectively, P is the Hill factor/slope factor or the inclination of the curve across log x_0. The Hill factor decides the gradient of a SDR plot and its value is unity for a standard SDR curve. The curve is reportedly steeper or shallow if the Hill factor value is more or less than 1, respectively[43]. After differentiating equation 3, the following equation is arrived at:

$$\frac{dy}{dx} = \frac{P \ln 10 (A_2 - A_1) 10^{(\log x_0 - x)P}}{\left\{1+10^{(\log x_0 - x)P}\right\}^2} \quad \text{.....(4)}$$

The differentiation, dy/dx, provides the maxima of curve and its value is found via. equalizing the differentiation i.e., d^2y / d^2x to zero, which leads to $x = log\ x_0$, Hence, $log\ x_0$ specifies the P_t in Eq. 3. Figure 6a shows the standard curve based on Eq. 3. Furthermore, the derivative curves, which were used to calculate the percolation threshold are presented in Fig. 6b-d and the values are reported along with other parameters in Table 3. The observations to note in these curves is that they are similar to Sigmoidal-Boltzmann model curves. The reason for this similarity is that the Y-axis value of S-B model resembles to S-DR model which is given as (A_1+A_2) / 2. Hence, the corresponding X-axis value at the Y-axis value i.e., (A_1+A_2) / 2 can be directly taken from the plots to get the percolation threshold. The inclination of the plot at $Y_{50}[(A_1+A_2)$ / 2] i.e., P indicates that the permittivity is highly enhanced near the P_t for all composites.

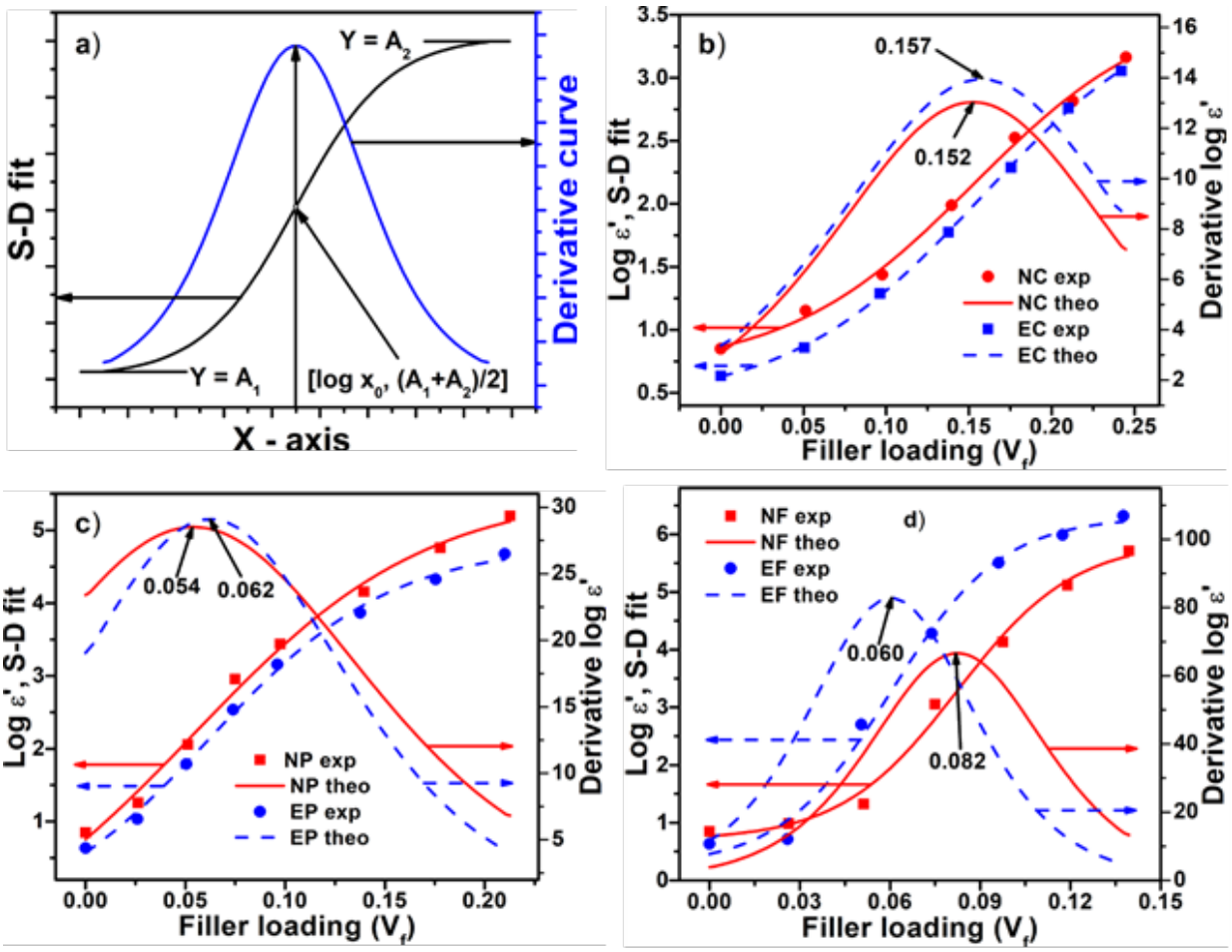

Fig. 6 Plots of (a) ideal curve (b) NC and EC composites (c) NP and EP composites, and (d) NF and EF composites based on experiment, theory and derivation as per SDR model

Table 3 Extracted data as per SDR model

SI	A_1	A_2	log x_0	P	x_0	R^2
NC	0.68±0.14	3.62±0.28	0.152±0.010	7.71±1.54	1.420	0.995
EC	0.42±0.05	3.68±0.11	0.157±0.003	7.43±0.48	1.436	0.999
NP	0.15±1.63	5.54±0.43	0.054±0.025	7.40±2.49	1.132	0.991
EP	0.08±0.55	4.80±0.17	0.062±0.009	9.54±1.67	1.154	0.995
NF	0.69±0.24	5.88±0.37	0.082±0.004	22.27±5.00	1.209	0.987
EF	0.24±0.37	6.31±0.26	0.060±0.003	23.72±4.98	1.149	0.988

Sigmoidal–Hill (SH) model

The SH model have been reportedly used in many applications such as sequestration of arsenite and chromium in nanostructured minerals such as ferrihydrite, siderite, and goethite[44], determine ethanol tolerance of probiotic yeast for use as functional beer[45], ascertain milk progesterone profile as a supplementary dataset to monitor reproduction status in cows[46], to enhance pharmacology and physiology related interpretability of modeled activity-pCa curves[47], and for prediction of deaths in the US due to COVID 19 pandemic[48], etc.

The Sigmoidal-Hill equation is given as below:

$$Y = A_1 + \frac{A_2 - A_1}{1 + \left(\frac{k}{x}\right)^n} \text{.....(5)}$$

where x is the independent parameter representing filler dosage volume fraction, Y is the dielectric permittivity at any value of x; A_1 and A_2 represent the permittivity of base polymer and the highest filler loaded composite, respectively, n is a coefficient, which represents the Hill factor and k is the filler quantity at condition $Y = (A_1+A_2) / 2$.

Simply rearranging the right-hand side of equation 5, it gets modified to:

$$Y = A_1 + (A_2 - A_1)\frac{x^n}{k^n + x^n} \text{.....(6)}$$

The derivative of equation 6 gives

$$\frac{dy}{dx} = (A_2 - A_1)\frac{nk^n x^{n-1}}{(k^n + x^n)^2} \text{.....(7)}$$

The P_t can be calculated through this model by equalizing d^2y / d^2x to 0 on the basis of the same arguments mentioned in above models and it leads us to the following equation.

$$x = k\left(\frac{n-1}{n+1}\right)^{\frac{1}{n}} \text{.....(8)}$$

Hence, the P_t depends upon the quantity n, where the Hill factor is greater than 1 and k, the amount of carbon fillers, which itself is dependent on A_1 and A_2. Upon inserting the values of x in Eq. 6, we get the next equation.

$$Y = \frac{A_1 k^n (n+1) + A_2 k(n-1)}{k^n (n+1) + k(n-1)} \text{.....(9)}$$

It provides the *Y*-axis parameter at percolation threshold. Figure 7a shows the standard curve as per the equation given above along with the derivative plots shown in Fig. 7b-d. The value of P_t has been calculated using the parameters of *k* and *n,* whose values are substituted in equation 8. The maxima of the above plots are employed to calculate the percolation threshold along with other calculated parameters as shown in Table 4. Interestingly, it is noted from Fig. 7 and Table 4 that the P_t values determined through the SH model are consistently less than both SB and SD models. The magnitude of the *Y*-axis parameter at Y_{50} for SB, SD and SH models is equal i.e., $(A_1 + A_2/2)$. On the contrary, the corresponding *X*-axis parameters represented in SB model, SD model, and SH model are x_0, $\log x_0$, and *k,* respectively. While these *X*-axis values in SB and SD models is indicating their P_t, but it is different for SH model as the parameter *k,* herein, is indicating the filler quantity at the condition $Y = (A_1+A_2)/2$. The percolation threshold, herein for SH model is represented by Eq. 8, that means it is always less than unity. Thus, the calculated values of percolation threshold via. SH model is always lower than other two models. Furthermore, *n* is the inclination near Y_{50} $[(A_1+A_2)/2]$. This indicates that permittivity has a high rate of increase around Y_{50} but not at P_t as both points differ from each other.

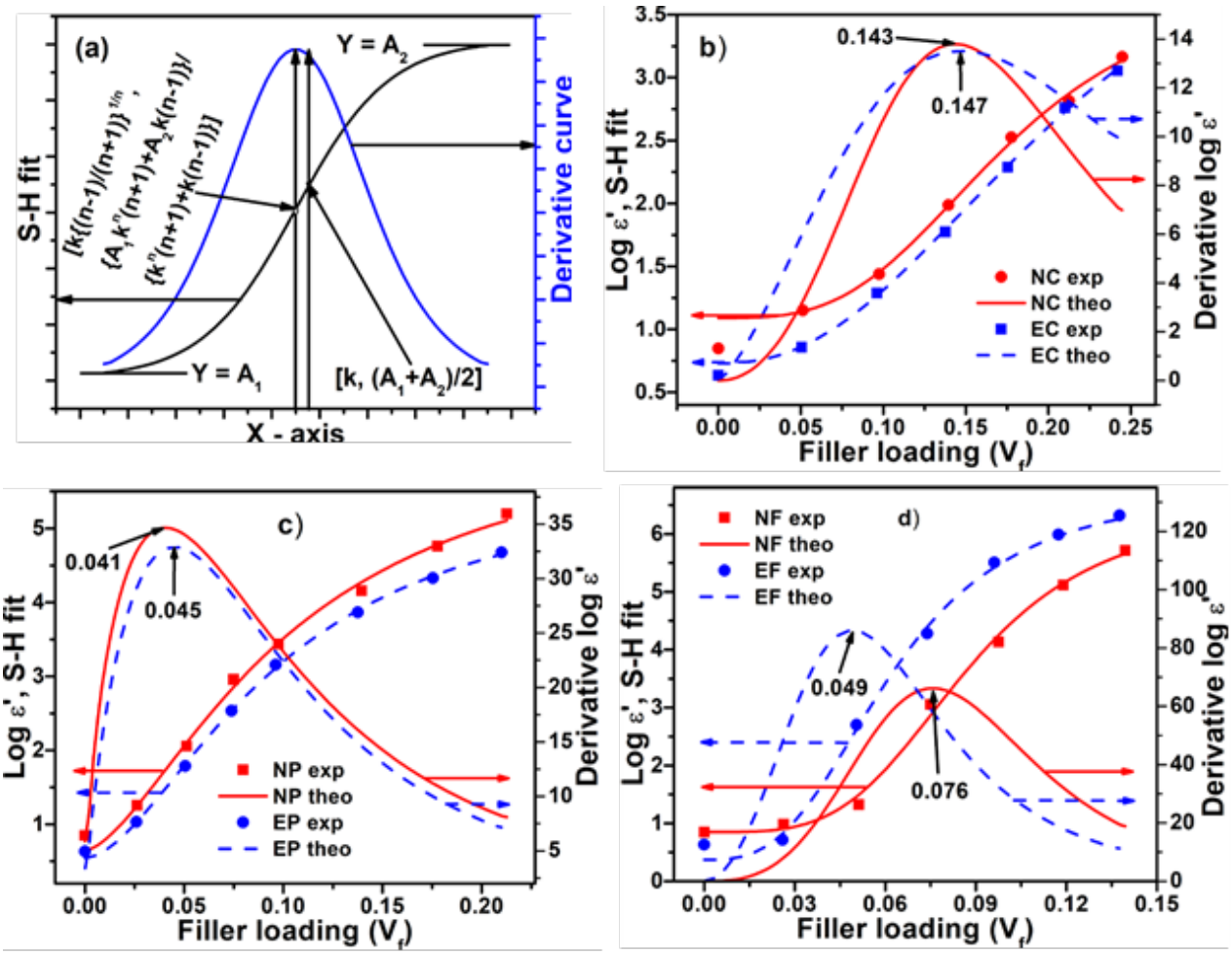

Fig. 7 Plots of (a) ideal curve (b) NC and EC composites (c) NP and EP composites, and (d) NF and EF composites based on experiment, theory and derivation as per SH model

Table 4 Extracted data as per SH model

SI	A_1	A_2	k	n	X_p	R^2
NC	1.098±0.21	3.853±1.15	0.1761±0.0479	3.1795±1.7199	0.143	0.973
EC	0.730±0.14	04.90±1.58	0.2178±0.0673	2.3339±0.7042	0.147	0.996
NP	0.648±0.59	06.52±1.35	0.1032±0.0232	1.5867±0.6304	0.041	0.993
EP	0.542±0.21	05.74±0.44	0.0975±0.0076	1.7193±0.2720	0.045	0.998
NF	0.849±0.19	06.43±0.58	0.0869±0.0056	3.8485±0.8065	0.076	0.993
EF	0.372±0.44	06.82±0.52	0.0623±0.0038	2.9579±0.7412	0.049	0.994

Sigmoidal–Logistic (SL) model

The SL model have been recently used in various applications such as accurately capturing the biological growth trajectory[49], evaluation of dry matter accumulation in triticale at west Anatolia, Turkey[50], to analyze genetically seed-filling technique in maize[51], fault diagnosis for planetary gearboxes of wind turbines[52], and model based discussion of COVID-19 pandemic in Asian countries,[53] etc.

This four-parameter model, can be represented with the following equation:

$$Y = A_1 + \frac{A_2 - A_1}{1 + (x/x_0)^P} \quad \text{..... (10)}$$

Where, Y is permittivity type response at the x value for loadings of carbons; A_1 and A_2 represent the permittivity of base polymer and the highest filler loaded sample, respectively; x_0 is midway between A_1 and A_2 having the same unit to x; and P is slope factor (>1) representing the gradient of a slope. The equalizing of d^2y / d^2x to 0 in the differentiated equation of equation 10 gives the below equation with RHS representing the percolation threshold:

$$x = x_0 \left(\frac{P-1}{P+1}\right)^{\frac{1}{P}} \quad \text{.....} \qquad (11)$$

On substituting x value from Eq. 11 into Eq. 10, we have the corresponding Y-axis value, which is given as below:

$$Y = \frac{A_1(P-1) + A_2(P+1)}{2P} \quad \text{..... (12)}$$

Figure 8a shows the ideal curve and Fig. 8b-d shows the plots of experimentally and theoretically obtained curves as per Eq. 10. The derivative curve of theoretical plot is also presented within the same figures. These derivative plots are employed to graphically determine the value of P_t for various composites. The percolation threshold obtained from the maxima of the plotted derivative curves have been mentioned in the Fig. 8b-d. By inserting the values of x_0 and P in Eq. 11, the calculated percolation threshold data along with other parameters have been mentioned in Table 5. It is observed that the percolation threshold value determined from the maxima of derivative curves and through the Eq. 11 have resembled with each other for a

particular composite. It is noticed that the values of percolation threshold of the SL model are always smaller than that of SB and SD models due to similar reasons explained in the discussions of SH model. Also, the percolation threshold calculated via. the S-L and SH models appear to be nearer but are unequal. The slope factor of the plot, P, is observed around Y_{50} $[(A_1+A_2)/2]$. This supports the basis that permittivity has a high rate of increase near Y_{50} but not around P_t as both points differ from each other. It is noticed from the table that P is greater than unity, which is in accordance with the statement of this model.

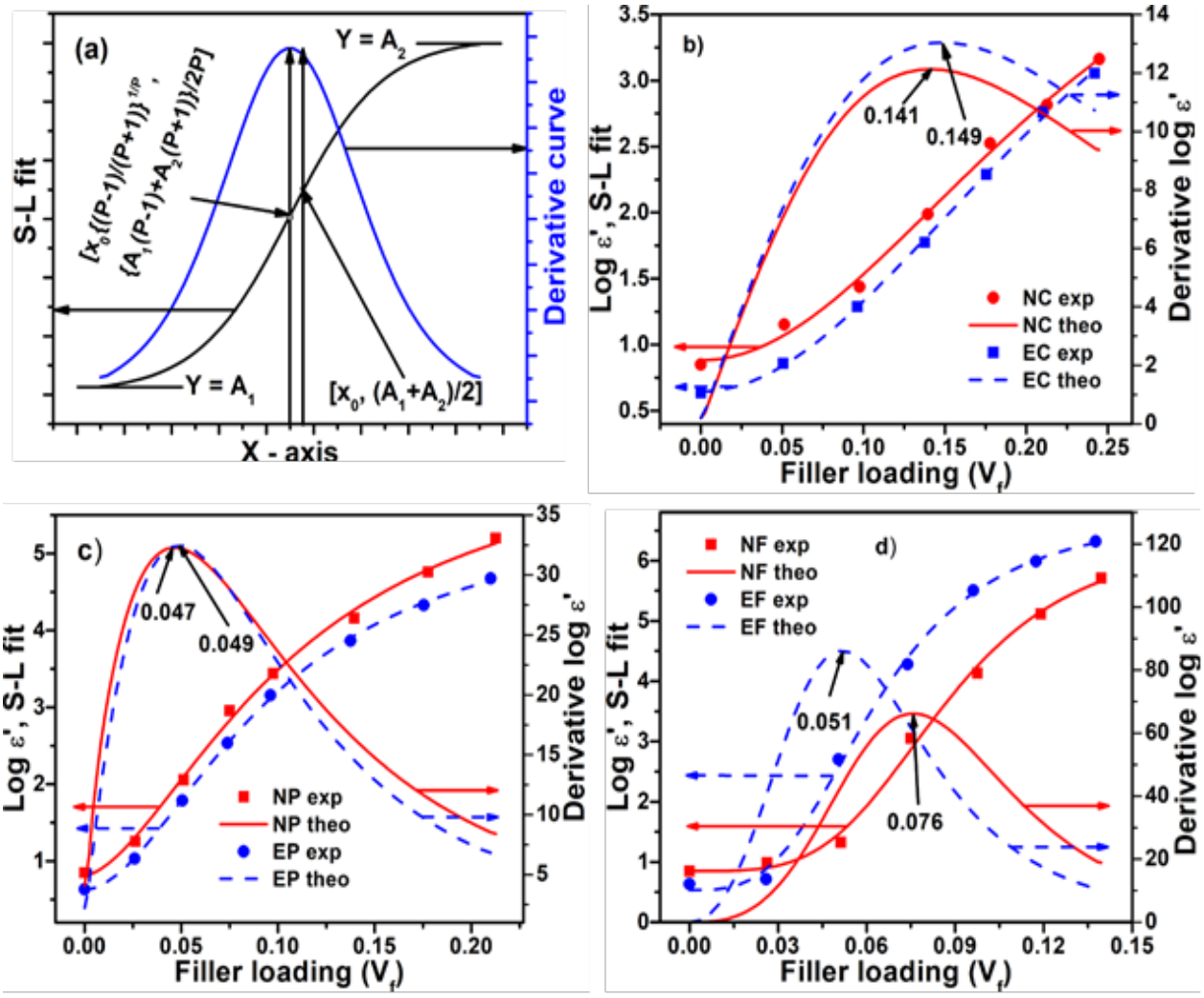

Fig. 8 Plots of (a) ideal curve (b) NC and EC composites (c) NP and EP composites, and (d) NF and EF composites based on experiment, theory and derivation as per SL model

Table 5 Extracted data as per SL model

SI	A_1	A_2	x_0	P	X_p	R^2
NC	0.88±0.07	5.44±1.98	0.244±0.101	2.00±0.47	0.141	0.992
EC	0.64±0.03	5.88±1.07	0.259±0.049	1.98±0.19	0.149	0.998
NP	0.81±0.09	6.56±0.59	0.108±0.015	1.65±0.21	0.047	0.996
EP	0.62±0.03	5.60±0.16	0.096±0.004	1.82±0.08	0.049	0.999
NF	0.84±0.12	6.43±0.55	0.086±0.006	3.84±0.70	0.076	0.992
EF	0.53±0.13	6.80±0.31	0.063±0.003	3.15±0.41	0.051	0.996

Sigmoidal–Logistic-1 (SL-1) model

The SL-1 model, also attributed as three-parameter model has been limited in terms of use for various applications. The first study on the model was taken up by Pierre Francois Verhulst for the investigation of increase in population of the human beings[54]. Other literature reporting the use of this model includes the growth of Lactococcus lactis in broth medium with varying conditions of aeration and agitation[55], loglet (logistic and wavelet) analysis for signal processing and compression to understand the effects of competitions within a market[56], and applications in COVID modelling[57–59]. The equation of SL-1 model is represented by:

$$Y = \frac{A_2}{1+ e^{-k\,(x- x_c)}} \quad \text{.....(13)}$$

Where, Y represents the permittivity at 'x' filler loading, A_2 is the upper (highest filler loading) values of permittivity, and k is a gradient. Moreover, x_c, herein, indicates the quantity of x at the sigmoidal midway. On differentiating Eq. 13, we have the following equation:

$$\frac{dy}{dx} = \frac{kA_2 e^{-k\,(x- x_c)}}{\left\{1+ e^{-k\,(x- x_c)}\right\}^2} \quad \text{.....(14)}$$

Furthermore, equating d^2y / d^2x to 0 gives us $x = x_c$. Thus, x_c in equation 14 expresses the P_t for SL-1 model. The replacement of x as x_c in Eq. 13, yields $Y = A_2/2$. A standard curve on the basis of SL-1 model is shown in Fig. 9a. However, Fig. 9b-d shows the curves plotted on the basis of experiment, theory, and theoretical derivation. The derivative curves are employed to graphically

determine the values of P_t for various composites. The P_t, taken from maxima of the derivative curves are mentioned within the graphs and these values along with other parameters are put in Table 6. From the table, figure and comparing the data with previously discussed models, it can be observed that the percolation threshold value for CCB filled NC and EC composites were the highest that are 0.192±0.051 and 0.181±0.022, respectively. In equation 12, the value of maxima for the permittivity is considered without giving much of a thought to the minima of the same while proposing this model. In contrast to the same, for any specific composite system, a minimum is also valued and hence more applicability of this model will be observed where the minima values equate to zero.

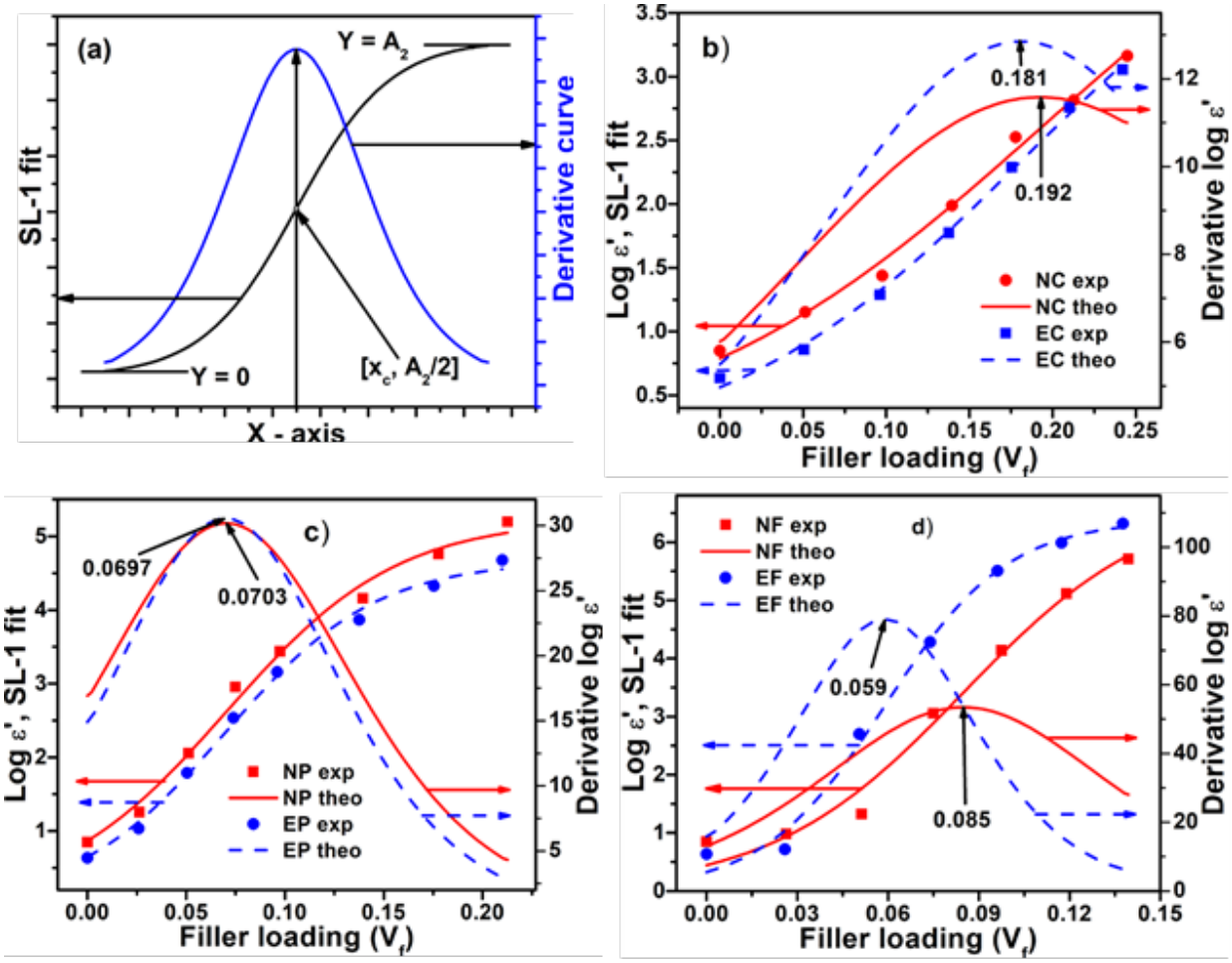

Fig. 9 Plots of (a) ideal curve (b) NC and EC composites (c) NP and EP composites, and (d) NF and EF composites based on experiment, theory and derivation as per SL-1 model

Table 6 Extracted data as per SL-1 model

SI	a	x_c	k	R^2
NC	5.18±1.13	0.192±0.051	8.9±1.4	0.990
EC	4.67±0.53	0.181±0.022	10.9±1.0	0.996
NP	5.24±0.18	0.0703±0.004	23.1±2.2	0.990
EP	4.67±0.10	0.0697±0.003	26.2±1.7	0.995
NF	6.81±0.94	0.085±0.012	31.3±6.2	0.975
EF	6.38±0.23	0.059±0.003	49.5±6.1	0.989

Classical percolation theory and models comparison

Shante and Kirkpatrick proposed the theory of the interaction of the properties of classical particles with a random medium, capable of showing critical behavior in a far simpler form. He attempted the development of concepts of percolation theory along with general characteristics related to the critical region about the start of percolation[60]. In the recent studies, it has been reportedly used for renormalization group theory for a time-varying network[61], landfill methane generation[62], electromagnetic shielding in polymer/MWCNT composites[63], COVID and other epidemics[64], etc.

The logarithmic form of equation based on the classical percolation theory can be:

$$log\ \varepsilon'_c = log\ \varepsilon'_0 + t \times \log(V_f - V_{fc}) \ldots\ldots\ldots (15)$$

Wherein, ε'_c is permittivity, V_f is filler quantity, V_{fc} is filler quantity at the percolation threshold, ε'_0 is a constant quantity with the dimension of permittivity, and t is a critical exponent. The value of t for a three-dimensional network is 1.65-2.0. In the above equation $V_f > V_{fc}$. The value of t and log ε'_0 can be obtained from the slope and intercept of the linear Eq. 15, when plotted log ε'_c vs. log $(V_f - V_{fc})$.

The graph of above *X-Y* plot is constructed for our polymeric composite systems by varying the V_{fc} values to exhibit the best linear fit. The exact value of percolation threshold is observed at the best fitting of plots as shown in Fig. 10a-b and the corresponding percolation threshold, t and R^2 values are given in Table 7. Figure 10a exhibits the permittivity curves against carbons' loadings for the composites. These plots are the same as that of seen in the fitting

curves of Sigmoidal models. The lowest values for percolation threshold are reported for fibrous carbon fillers followed by PCB and CCB filled polymeric composites. This is attributed to the structure of carbon materials as discussed in our earlier publication[31]. The lowest percolation threshold in short carbon fiber composites is due to the low breakdown of fibres owing to the high aspect ratio and subsequent network formation. Conductex carbon black filler is having low structure, thus show high value of Pt. Conversely, for printex carbon black filler, the structure is very large and thus it exhibits lower percolation threshold than conductex black. When compared the Sigmoidal models, the P_t determined via classical theory are consistently the lowest of all. This lower value of P_t for classical theory is owing to higher value of critical exponent i.e. higher slope value[65]. The permittivity increment rate is dependent upon the gradient change with respect to the variation in the filler. A higher increase in the permittivity with an increase in filler concentration results in higher slope values. As seen in Fig. 10a-b, EF possesses slightly higher slope compared to NP with respect to the rate of increment.

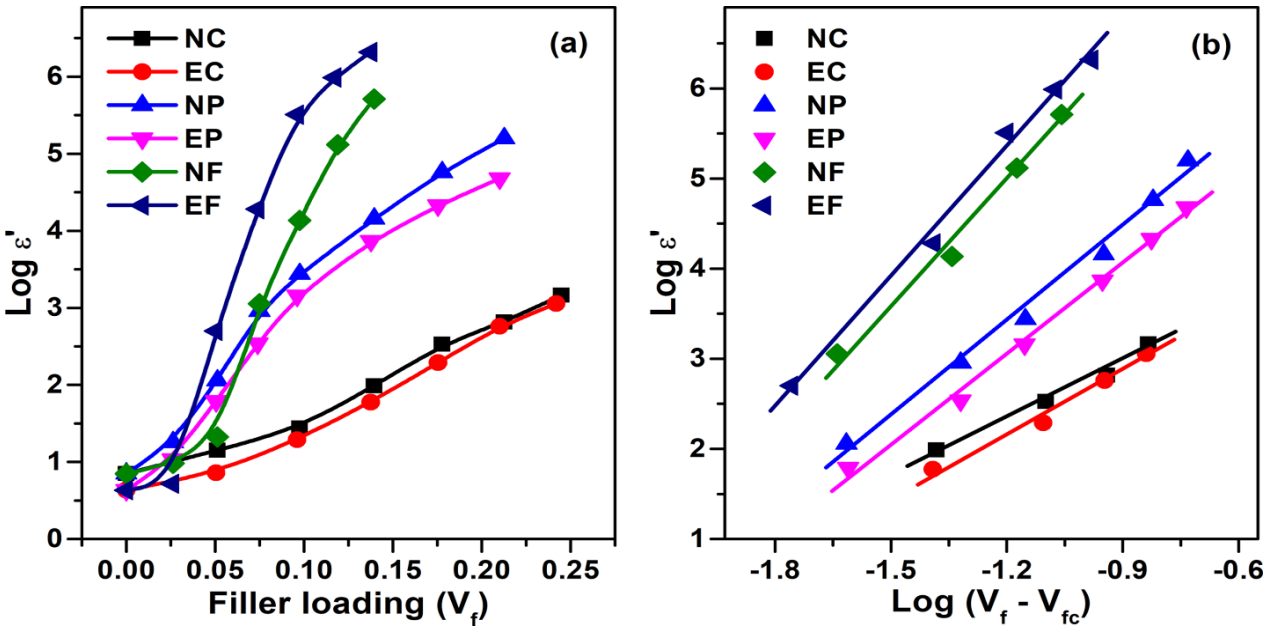

Fig. 10 Plots of (a) dielectric constant vs filler loading and (b) dielectric constant as per classical theory

Table 7 Extracted data percolation threshold as per classical theory

SI	R^2	Slope	Intercept	Percolation Threshold
NC	0.981	2.07±0.16	4.83± 0.18	0.098
EC	0.977	2.31±0.21	4.95±0.22	0.097
NP	0.987	3.51±0.18	7.62±0.20	0.027
EP	0.993	3.35±0.13	7.07±0.14	0.026
NF	0.982	4.59±0.37	10.48±0.49	0.052
EF	0.991	4.80±0.23	11.10±0.30	0.033

For the betterment of readers, the experimental (herein classical) and predicted percolation thresholds values from all Sigmoidal models are shown in Table 8, which will help to compared the data of percolation thresholds too easily.

Table 8 Values of all percolation thresholds determined experimentally as well as Sigmoidal models

SI	Percolation Threshold Values					
	Classical	SB	SD	SH	SL	SL1
NC	0.098	0.152	0.152	0.143	0.141	0.192
EC	0.097	0.157	0.157	0.147	0.149	0.181
NP	0.027	0.054	0.054	0.041	0.047	0.0703
EP	0.026	0.062	0.062	0.045	0.049	0.0697
NF	0.052	0.082	0.082	0.076	0.076	0.085
EF	0.033	0.060	0.060	0.049	0.051	0.059

Test of models on permittivity data of other publications

With the discussions till now, the potential of different sigmoidal models for the percolation threshold determination can be well comprehended. An attempt has been made to test these models for other polymeric composites to check their applicable relevancy, and hence, the percolation threshold obtained were compared with published literature[11, 22, 66, 67]. The filler

loading and permittivity have been converted into volume fraction and log ε', respectively. The data of permittivity, taken from the above mentioned references are for polyvinylidenefluoride (PVDF)/carbon/MWCNTs nanocomposite, epoxy/r-GO/carbon black nanocomposite, polyethylene (LDPE and LLDPE)/carbon black nanocomposites, and PVDF/carbon/silica nanohybrid nanocomposites, respectively. The results of these literature along with their sigmoidal fitting curves and their derivative ones are reported in Fig. 11a-d and the respective data is collectively tabulated and represented in Table 9.

It is observed from Fig. 11a-c that the rate of increment of permittivity is less. Furthermore, Fig. 11c is indicative of it shifting towards the left side of the curve. Figure 11a and d indicate that the different Sigmoidal models barring SL-1 model are applicable and fitting well. They are valid thereby providing us with the values for the percolation threshold for the permittivity. The SL-1 model is not valid as a function of its non-sigmoidal nature as observed with the visible non-exponential behavior. Due to the same, the highest and lowest values of permittivity i.e., A_1 and A_2 are absent. Also, the difference between other model values with the SL-1 model values for all four reported models is very high. However, if higher filler concentrations are tested along with more testing carried out over the same, there may be a chance for it to be sigmoidal at a higher filler loading percentage. On the other hand, Fig. 11d is observed to be shifting towards the right side of the curve. It also indicates the highest values of filler concentration required to reach the P_t value. The rate of increment for permittivity is observed to be lower at the start, medium in the mid-range, and lower again at the end part of the curve thereby giving it a bell-shaped form.

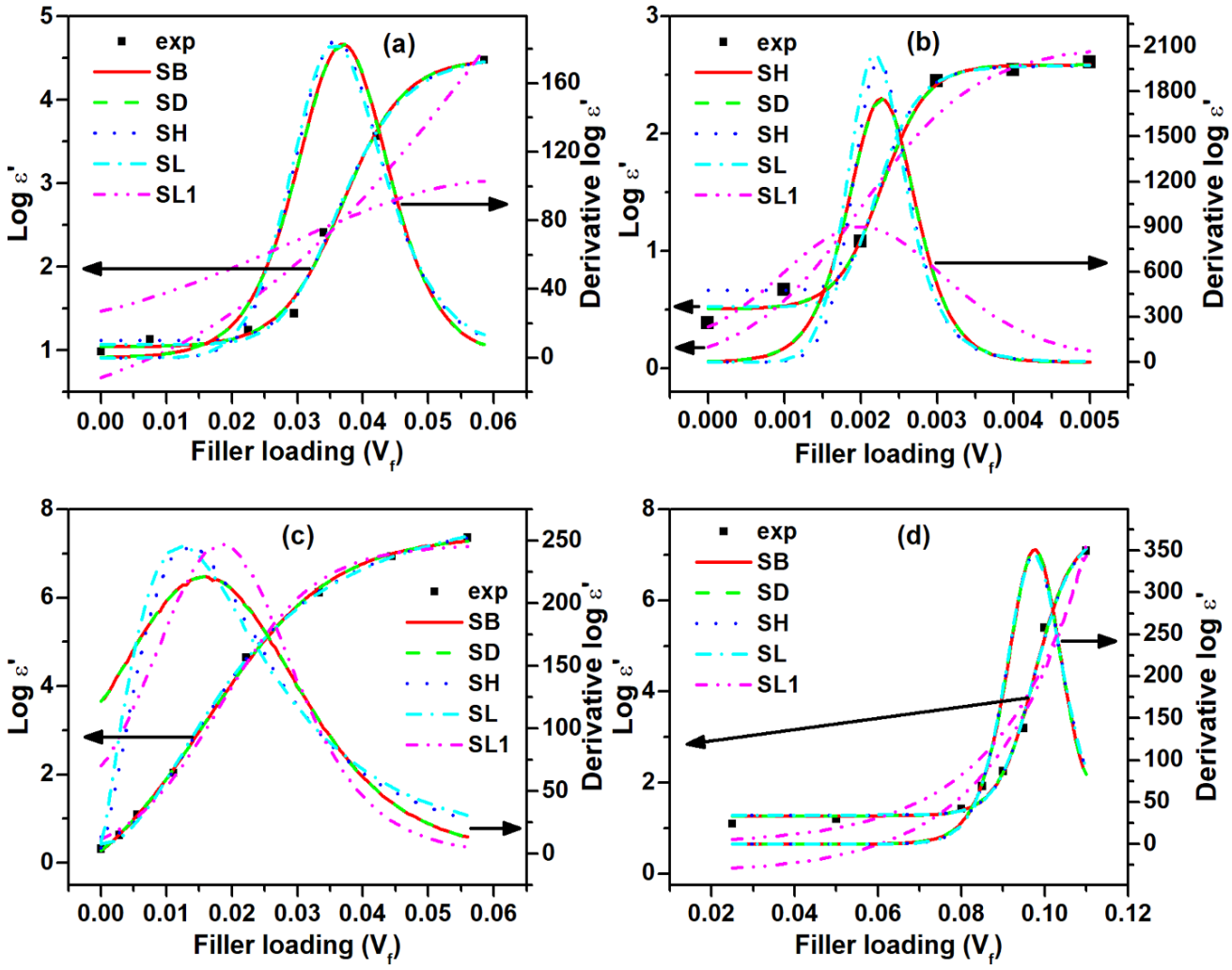

Fig. 11 Test of different models on permittivity data taken from other publications a) [66], b) [11], c) [22], and d) [67] based on different sigmoidal models

Table 9 Percolation threshold as per different models

SI	Percolation threshold (Vfc)				
	SB	SD	SH	SL	SL1
(a) [66]	0.0376	0.0376	0.0365	0.0352	-------
(b) [11]	0.0023	0.0023	0.0022	0.0021	0.002
(c) [22]	0.0158	0.0158	0.0135	0.0124	0.018
(d) [67]	0.0976	0.0976	0.0971	0.0971	-------

Conclusions

The σ, ε′ and ε″ have increased with the increase in carbon fillers' concentration. NBR composites showed higher AC conductivity and dielectric properties compared to EVA ones for both type of black filled composites. However, the fiber filled system exhibits opposite trend that is higher AC conductivity and dielectric properties for EVA filled systems compared to NBR ones. This is mainly due to viscosity of the system during mixing. The level of σ, ε′ and ε″ imparted by different carbon fillers is in the order SCF> Printex black> Conductex black. The values of ε′ and ε″ for the composites, having lower carbons' loadings are frequency independent in nature. However, for all composites, having permittivity above percolation threshold, the values of ε′ and ε″ have reduced when the frequency is proceeded to its higher value. The percolation threshold has been determined with the use of various sigmoidal models based on the highest value of permittivity increase rate. The percolation threshold of permittivity was determined using different Sigmoidal models such as SB, SDR, SH, SL, SL-1, and classical percolation theory but we observed almost similar values for SB and SD models. This can be attributed to the corresponding equal value of *Y*-axis parameter that is $(A_1 + A_2)/2$. The percolation threshold value of the composites determined using SH and SL models are not very different from each other but are certainly lower than that of SB and SD models for the present study. When compared, the percolation threshold value, determined with the help of classical theory is consistently the lowest of all other models. The value of coefficient of correlation (R^2) close to unity indicates the proper validity of these models. Accordingly, SH and SL-1 models are not properly valid for NC and NF composites. These Sigmoidal models, as tested for other polymer composites from published literature revealed that except SL-1 model, all other models can be consistently utilized to determine the percolation threshold of permittivity for polymer composite systems. In case of high filler loadings in polymer composites, this study can be vital in determining the required filler quantity to get the desire level of permittivity. This in turn could save all resources (5 M's) i.e., machine, money, material, method, and manpower that will have to be invested to experimentally reach to the desirable percolation threshold values. Finally, several orders of improvement in dielectric permittivity suggest that these composites can be used for supercapacitor application.

Declarations

Ethics approval and consent to participate N/A

Consent for publication N/A

Availability of data and material Data are available on request to the corresponding author.

Competing interests The authors declare no competing of financial interest.

Funding This work is funded by the Researchers Supporting Project number (RSPD2023R674), King Saud University, Riyadh, Saudi Arabia.

Authors' contributions MR has given the idea of the work, conducted experiments, and analysed the data. MR and PG along with all other authors have mostly contributed in writing the manuscript. All the authors have agreed to the submission of final version of the manuscript.

Acknowledgements The authors acknowledge the Researchers Supporting Project number (RSPD2023R674), King Saud University, Riyadh, Saudi Arabia for funding this research work.

ORCID *Mostafizur Rahaman* https://orcid.org/0000-0002-5495-1771

References

1. Chu B, Zhou X, Ren K, et al (2006) A dielectric polymer with high electric energy density and fast discharge speed. Science 313:334–336
2. Guo B, Ma PX (2018) Conducting polymers for tissue engineering. Biomacromolecules 19:1764–1782
3. Yang Z, Gao F, Du H, et al (2019) Grain size engineered lead-free ceramics with both large energy storage density and ultrahigh mechanical properties. Nano Energy 58:768–777
4. Trukhanov SV, Trukhanov AV, Salem MM, et al (2018) Preparation and investigation of structure, magnetic and dielectric properties of (BaFe11. 9Al0. 1O19) 1-x-(BaTiO3) x bicomponent ceramics. Ceram Int 44:21295–21302
5. Shan X, Zhang L, Wu P, et al (2008) Dielectric response of ceramic-polymer composite with high permittivity. MRS Online Proc Libr Arch 1134:
6. Chen R-C, Zhang Q-P, Ke K, et al (2020) Chemically bonding BaTiO3 nanoparticles in highly filled polymer nanocomposites for greatly enhanced dielectric properties. J Mater Chem C 8:8786–8795. https://doi.org/10.1039/D0TC01296C

7. Jin Y, Xia N, Gerhardt RA (2016) Enhanced dielectric properties of polymer matrix composites with BaTiO3 and MWCNT hybrid fillers using simple phase separation. Nano Energy 30:407–416
8. Hosier IL, Praeger M, Vaughan AS, Swingler SG (2015) Electrical properties of polymer nano-composites based on oxide and nitride fillers. In: 2015 IEEE Electrical Insulation Conference (EIC). IEEE, pp 438–441
9. Nilagiri Balasubramanian KB, Ramesh T (2018) Role, effect, and influences of micro and nano-fillers on various properties of polymer matrix composites for microelectronics: A review. Polym Adv Technol 29:1568–1585
10. Panda M, Srinivas V, Thakur A (2008) On the question of percolation threshold in polyvinylidene fluoride/nanocrystalline nickel composites. Appl Phys Lett 92:132905
11. Huang T, Ma C-G, Dai P-B, Zhang J (2019) Improvement in dielectric constant of carbon black/epoxy composites with separated structure by surface-modified hollow glass beads with reduced graphene oxide. Compos Sci Technol 176:46–53
12. Forintos N, Czigany T (2019) Multifunctional application of carbon fiber reinforced polymer composites: electrical properties of the reinforcing carbon fibers–a short review. Compos Part B Eng 162:331–343
13. Wu W, Zhao W, Sun Q, et al (2020) Surface treatment of two dimensional MXene for poly(vinylidene fluoride) nanocomposites with tunable dielectric permittivity. Compos Commun 100562. https://doi.org/10.1016/j.coco.2020.100562
14. Collins I, Hossain M, Dettmer W, et al Flexible membrane structures for wave energy harvesting: A review of the developments, materials and computational modelling approaches. Artic Press Renew Sustain Energy Rev 1–49
15. Panda M (2023) Percolation, Scaling, and Relaxation in Polymer Dielectrics. Springer Nature
16. Fahim M, Bijwe J, Nalwa HS (2001) Chapter 8 - Polyimides for Microelectronics and Tribology Applications. In: Nalwa HS (ed) Supramolecular Photosensitive and Electroactive Materials. Academic Press, San Diego, pp 643–726
17. Panda M, Srinivas V, Thakur A (2008) Surface and interfacial effect of filler particle on electrical properties of polyvinyledene fluoride/nickel composites. Appl Phys Lett 93:242908
18. Panda M, Srinivas V, Thakur A (2011) Role of polymer matrix in large enhancement of dielectric constant in polymer-metal composites. Appl Phys Lett 99:042905
19. Panda M (2017) Major role of process conditions in tuning the percolation behavior of polyvinylidene fluoride based polymer/metal composites. Appl Phys Lett 111:082901
20. Panda M (2021) Tuned dielectric and percolation behavior of cold-pressed polyvinyledene fluoride nanocomposites caused by Ni and BaTiO 3 fillers. Indian J Phys 1–5
21. Panda M, Srinivas V, Thakur A (2015) Non-universal scaling behavior of polymer-metal composites across the percolation threshold. Results Phys 5:136–141
22. Rahaman M, Al Ghufais IA, Periyasami G, Aldalbahi A (2020) Recycling and Reusing Polyethylene Waste as Antistatic and Electromagnetic Interference Shielding Materials. Int J Polym Sci 2020:

23. Ram R, Rahaman M, Khastgir D (2013) Mechanical, electrical, and dielectric properties of polyvinylidene fluoride/short carbon fiber composites with lowelectrical percolation threshold. J APPL POLYM SCI 10
24. El Aferni A, Guettari M, Tajouri T (2020) Mathematical model of Boltzmann's sigmoidal equation applicable to the spreading of the coronavirus (Covid-19) waves. Environ Sci Pollut Res 1–9
25. Zanatta AR (2019) Revisiting the optical bandgap of semiconductors and the proposal of a unified methodology to its determination. Sci Rep 9:1–12
26. Mance D, Wiese R, Kewitz T, Kersten H (2018) Atmospheric pressure plasma jet for biomedical applications characterised by passive thermal probe. Eur Phys J D 72:98
27. Cruz KA, Juárez JM, Álvarez MZ, et al (2020) Modeling of the chemical x-parameter in pseudobinary alloys from the shift of the x-ray bragg angle: Application to cubic BaxSr1-xTiO3 films. Dig J Nanomater Biostructures 15:33–40
28. Gokhfeld D (2018) Use of a sigmoid function to describe second peak in magnetization loops. J Supercond Nov Magn 31:1785–1789
29. Gondaliya N, Kanchan DK, Sharma P, Jayswal MS (2012) Dielectric and electric properties of plasticized PEO-AgCF3SO3-SiO2 nanocomposite polymer electrolyte system. Polym Compos 33:2195–2200
30. Nayak S, Rahaman M, Pandey AK, et al (2013) Development of poly(dimethylsiloxane)-titania nanocomposites with controlled dielectric properties: Effect of heat treatment of titania on electrical properties. J Appl Polym Sci 127:784–796. https://doi.org/10.1002/app.37777
31. Rahaman M, Chaki TK, Khastgir D (2011) Development of high performance EMI shielding material from EVA, NBR, and their blends: effect of carbon black structure. J Mater Sci 46:3989–3999. https://doi.org/10.1007/s10853-011-5326-x
32. Rahaman M, Thomas SP, Hussein IA, De SK (2013) Dependence of electrical properties of polyethylene nanocomposites on aspect ratio of carbon nanotubes. Polym Compos 34:494–499. https://doi.org/10.1002/pc.22447
33. He F, Lau S, Chan HL, Fan J (2009) High dielectric permittivity and low percolation threshold in nanocomposites based on poly (vinylidene fluoride) and exfoliated graphite nanoplates. Adv Mater 21:710–715
34. Dang Z-M, Wang L, Yin YI, et al (2007) Giant dielectric permittivities in functionalized carbon-nanotube/electroactive-polymer nanocomposites. Adv Mater 19:852–857
35. Rahaman M, Chaki TK, Khastgir D (2011) High-performance EMI shielding materials based on short carbon fiber-filled ethylene vinyl acetate copolymer, acrylonitrile butadiene copolymer, and their blends. Polym Compos 32:1790–1805. https://doi.org/10.1002/pc.21212
36. Krupa I, Chodak I (2001) Physical properties of thermoplastic/graphite composites. Eur Polym J 37:2159–2168
37. Yang L, Schruben DL (1994) Electrical resistivity behavior of mold-cast metal-filled polymer composites. Polym Eng Sci 34:1109–1114
38. Rahaman M, Chaki TK, Khastgir D (2012) Determination of percolation limits of conductivity, dielectric constant, and EMI SE for conducting polymer composites using Sigmoidal Boltzmann model. Adv Sci Lett 10:115–117

39. Alevronta E, Skokic V, Wilderäng U, et al (2018) Dose-response relationships of the sigmoid for urgency syndrome after gynecological radiotherapy. Acta Oncol 57:1352–1358
40. Schneider U, Ernst M, Hartmann M (2017) The dose-response relationship for cardiovascular disease is not necessarily linear. Radiat Oncol 12:1–4
41. Rahmatpour S, Shirvani M, Mosaddeghi MR, et al (2017) Dose–response effects of silver nanoparticles and silver nitrate on microbial and enzyme activities in calcareous soils. Geoderma 285:313–322
42. Jeon S, Ko M, Lee J, et al (2020) Identification of Antiviral Drug Candidates against SARS-CoV-2 from FDA-Approved Drugs. Antimicrob Agents Chemother 64:. https://doi.org/10.1128/AAC.00819-20
43. Macdougall J (2006) Analysis of dose–response studies—E max model. In: Dose finding in drug development. Springer, pp 127–145
44. Hajji S, Montes-Hernandez G, Sarret G, et al (2019) Arsenite and chromate sequestration onto ferrihydrite, siderite and goethite nanostructured minerals: Isotherms from flow-through reactor experiments and XAS measurements. J Hazard Mater 362:358–367
45. Ramírez-Cota GY, López-Villegas EO, Jiménez-Aparicio AR, Hernández-Sánchez H (2020) Modeling the Ethanol Tolerance of the Probiotic Yeast Saccharomyces cerevisiae var. boulardii CNCM I-745 for its Possible Use in a Functional Beer. Probiotics Antimicrob Proteins 1–8
46. Adriaens I, Huybrechts T, Geerinckx K, et al (2017) Mathematical characterization of the milk progesterone profile as a leg up to individualized monitoring of reproduction status in dairy cows. Theriogenology 103:44–51. https://doi.org/10.1016/j.theriogenology.2017.07.040
47. Rockenfeller R, Günther M (2017) Hill equation and Hatze's muscle activation dynamics complement each other: enhanced pharmacological and physiological interpretability of modelled activity-pCa curves. J Theor Biol 431:11–24. https://doi.org/10.1016/j.jtbi.2017.07.023
48. Aboelkassem Y (2020) COVID-19 pandemic: A Hill type mathematical model predicts the US death number and the reopening date. medRxiv
49. Cao L, Shi P-J, Li L, Chen G (2019) A New Flexible Sigmoidal Growth Model. Symmetry 11:204. https://doi.org/10.3390/sym11020204
50. Hocaoğlu O, Coşkun Y (2018) Evaluation of dry matter accumulation in triticale by different sigmoidal growth models in west anatolia of turkey. Genetika 50:561–574
51. Yin S, Li P, Xu Y, et al (2020) Genetic and genomic analysis of the seed-filling process in maize based on a logistic model. Heredity 124:122–134
52. Qin Y, Wang X, Zou J (2018) The optimized deep belief networks with improved logistic Sigmoid units and their application in fault diagnosis for planetary gearboxes of wind turbines. IEEE Trans Ind Electron 66:3814–3824
53. Aviv-Sharon E, Aharoni A (2020) Generalized logistic growth modeling of the COVID-19 pandemic in Asia. Infect Dis Model 5:502–509
54. Verhulst PF (1838) Notice sur la loi que la population poursuit dans son accroissement. Corresp Mathématique Phys 10:113–121

55. Singh S, Singh KN, Mandjiny S, Holmes L (2015) Modeling the Growth of Lactococcus lactis NCIM 2114 under Differently Aerated and Agitated Conditions in Broth Medium. Fermentation 1:86–97. https://doi.org/10.3390/fermentation1010086
56. Meyer PS, Yung JW, Ausubel JH (1999) A Primer on Logistic Growth and Substitution: The Mathematics of the Loglet Lab Software. Technol Forecast Soc Change 61:247–271. https://doi.org/10.1016/S0040-1625(99)00021-9
57. Postnikov EB (2021) Reproducing country-wide COVID-19 dynamics can require the usage of a set of SIR systems. PeerJ 9:e10679
58. Postnikov EB (2020) Estimation of COVID-19 dynamics "on a back-of-envelope": Does the simplest SIR model provide quantitative parameters and predictions? Chaos Solitons Fractals 135:109841
59. Dattoli G, Di Palma E, Licciardi S, Sabia E (2020) On the evolution of covid-19 in italy: a follow up note. ArXiv Prepr ArXiv200312667
60. Shante VK, Kirkpatrick S (1971) An introduction to percolation theory. Adv Phys 20:325–357
61. Karschau J, Zimmerling M, Friedrich BM (2018) Renormalization group theory for percolation in time-varying networks. Sci Rep 8:8011. https://doi.org/10.1038/s41598-018-25363-2
62. Aranda-de La Teja C, Domínguez-Ortiz A (2020) application of percolation theory and fractal geometry to landfill methane production. Rev Mex Ing Quím 19:205–214
63. Shi Y-D, Li J, Tan Y-J, et al (2019) Percolation behavior of electromagnetic interference shielding in polymer/multi-walled carbon nanotube nanocomposites. Compos Sci Technol 170:70–76
64. Mello IF, Squillante L, Gomes GO, et al (2020) Epidemics, the Ising-model and percolation theory: a comprehensive review focussed on Covid-19. ArXiv Prepr ArXiv200311860
65. Rahaman M, Aldalbahi A, Govindasami P, et al (2017) A New Insight in Determining the Percolation Threshold of Electrical Conductivity for Extrinsically Conducting Polymer Composites through Different Sigmoidal Models. Polymers 9:527. https://doi.org/10.3390/polym9100527
66. Xue Q, Guo Q, Tao B, et al (2017) Ultrahigh permittivity of polymer nanocomposites based on surface-modified amorphous carbon/MWCNTs shell/core structured nanohybrids. Compos Part Appl Sci Manuf 100:324–332
67. Lei T, Xue Q, Chu L, et al (2013) Excellent dielectric properties of polymer composites based on core-shell structured carbon/silica nanohybrid. Appl Phys Lett 103:012902